Electronic Supplementary Material (ESI) for Journal of Materials Chemistry A.

Supporting Information

Graphene nanodots and oxygen defects incorporation triggers robust energy coupling between solar and reactive oxygen

YuchenHao, Xiaoli Dong*, Xiuying, Wang, Hongchao Ma,and Xiufang Zhang

School of Light Industry and Chemical Engineering, Dalian Polytechnic University, Dalian,Liaoning, 116034, P.R. China.

**Corresponding author. E-mail: dongxl@dlpu.edu.cn*

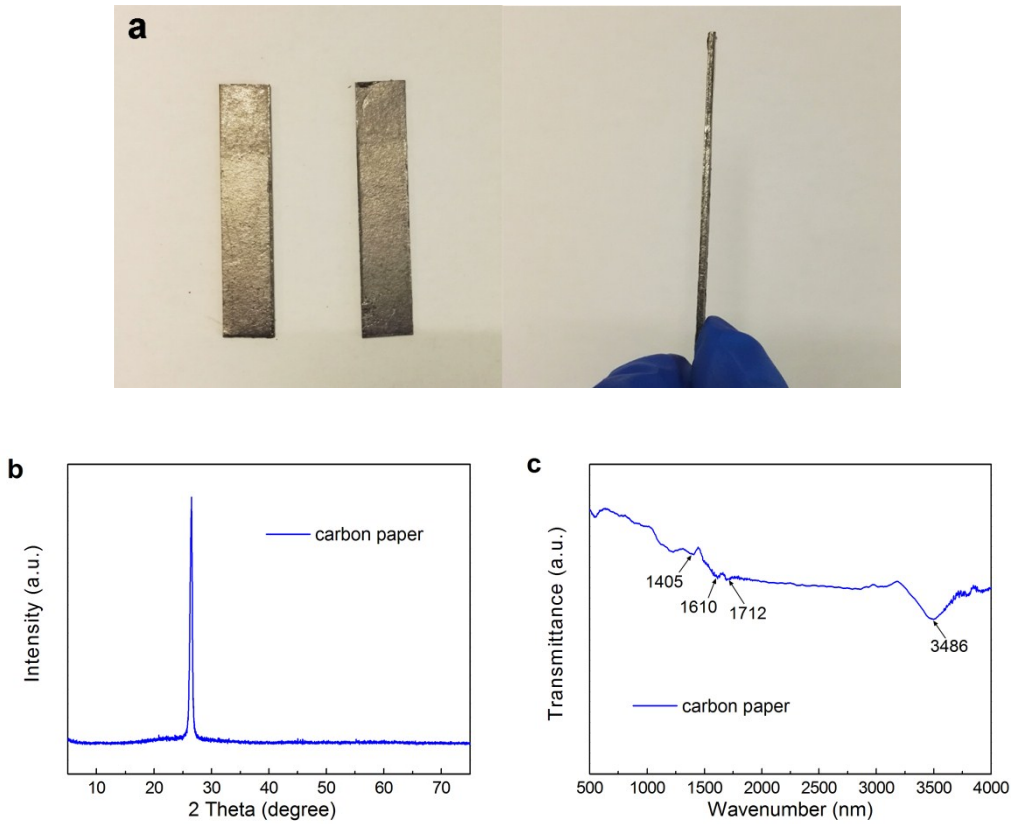

Fig. S1. The photographs (a), XRD pattern (b) and FT-IR spectra (c) of carbon paper.

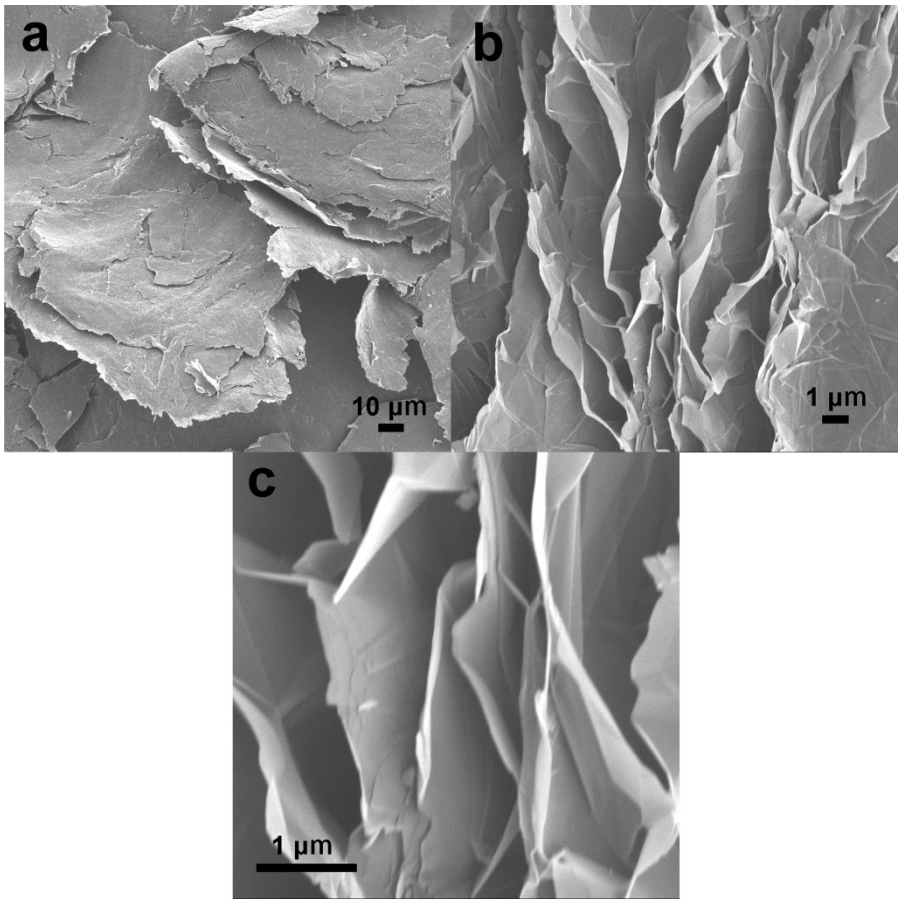

Fig. S2. The SEM images of carbon paper.

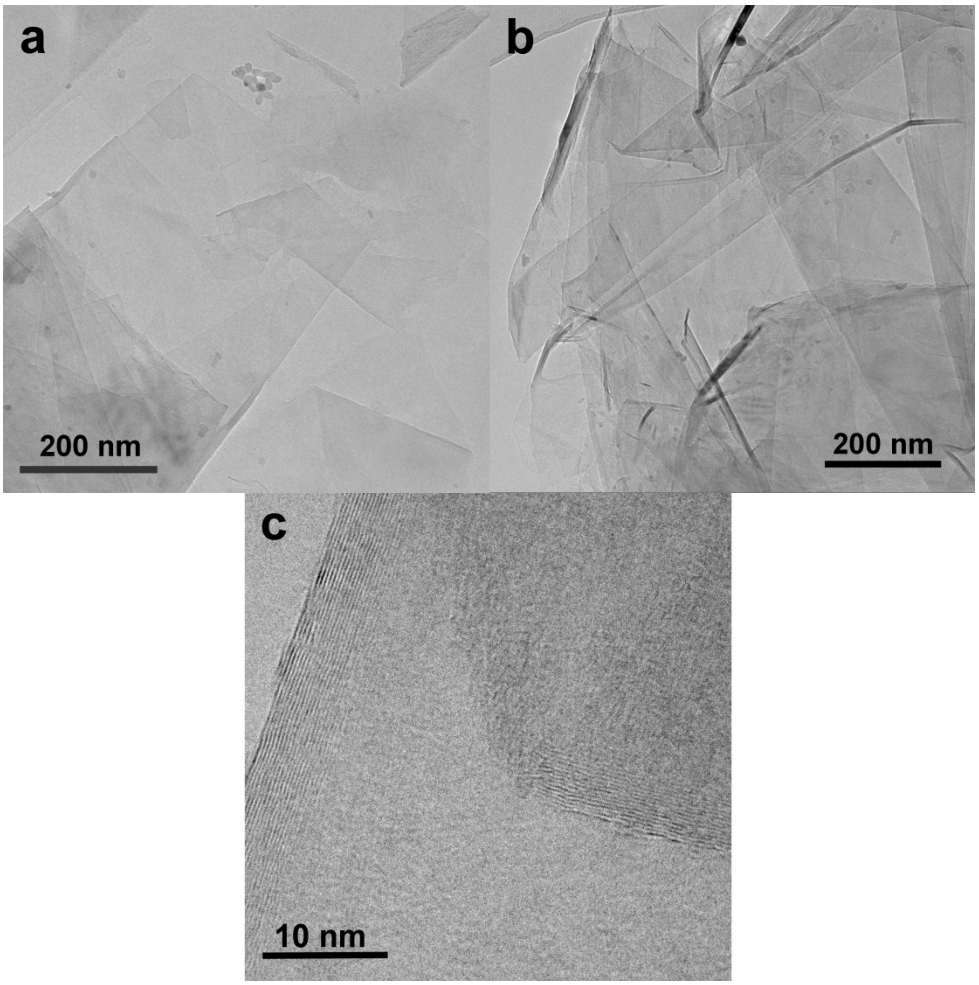

Fig. S3. (a)-(b) TEM images, (c) HRTEM image.

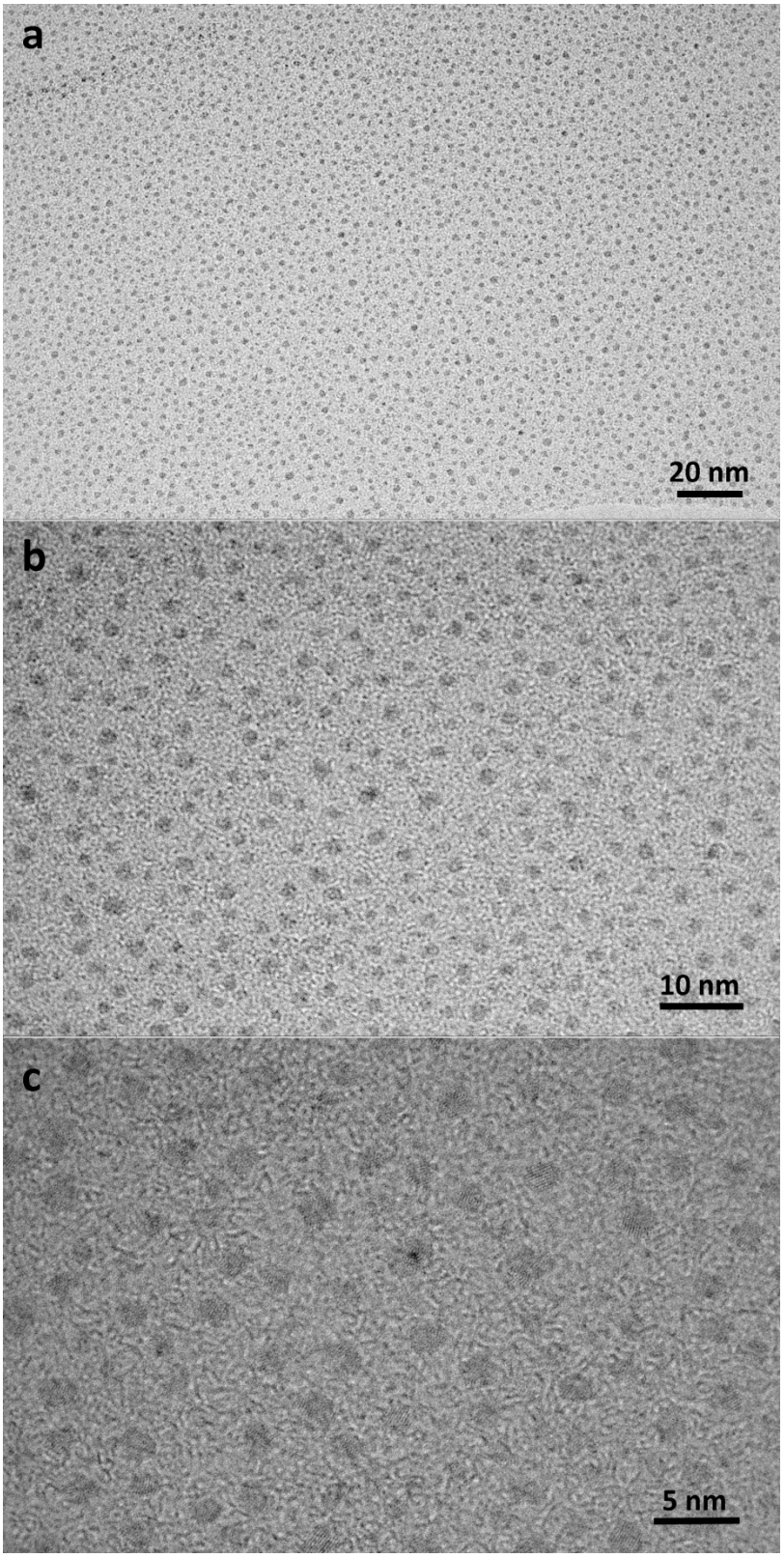

Fig. S4. TEM images of the as-prepared GDs.

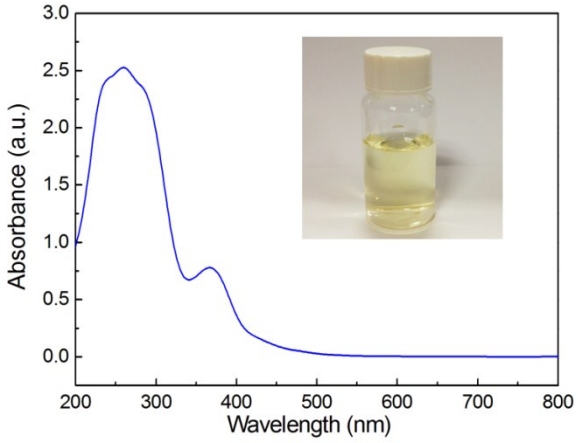

Fig. S5. Ultraviolet-visible spectra of the as-prepared GDs.

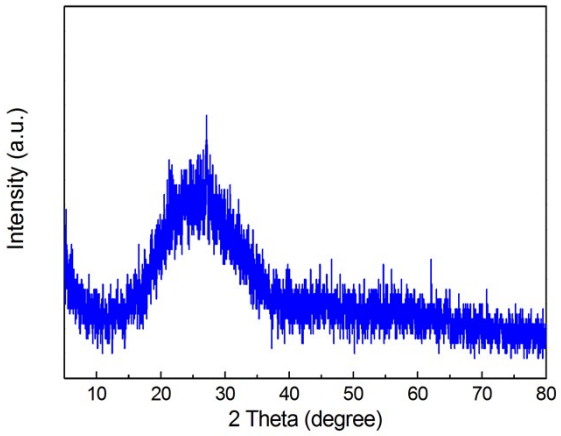

Fig. S6. XRD pattern of the as-prepared GDs.

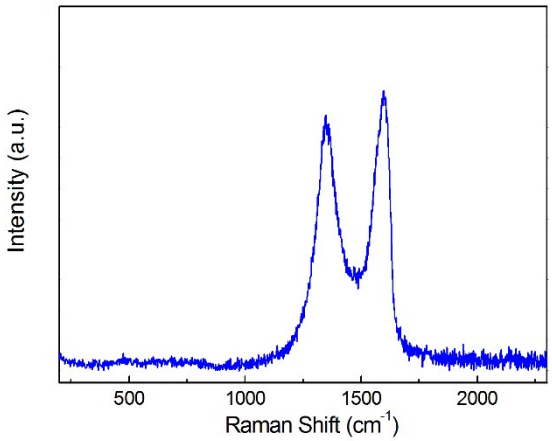

Fig. S7. Raman spectra of the as-prepared GDs.

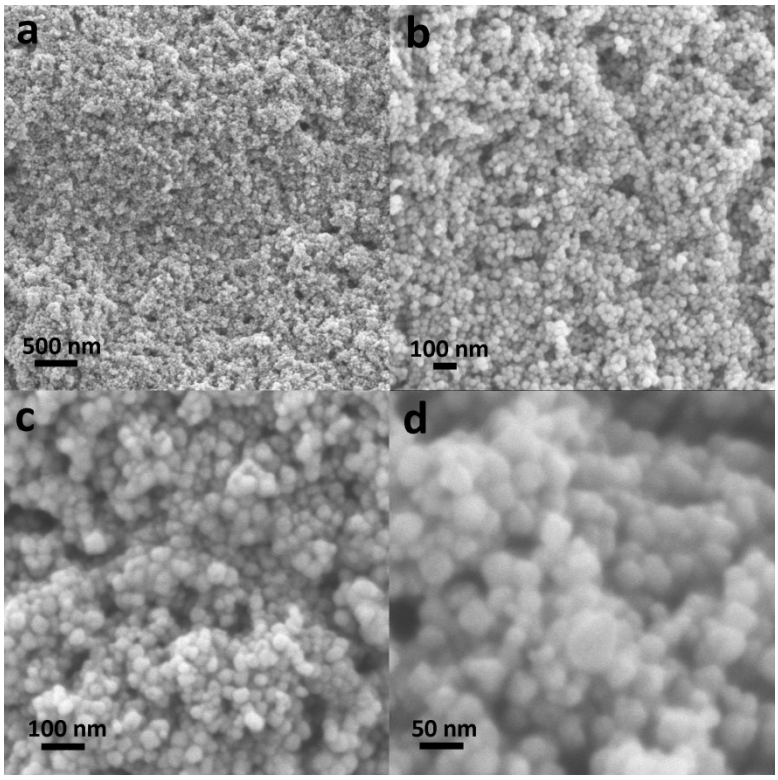

Fig. S8. SEM images of the pure TiO_2 catalyst (P25).

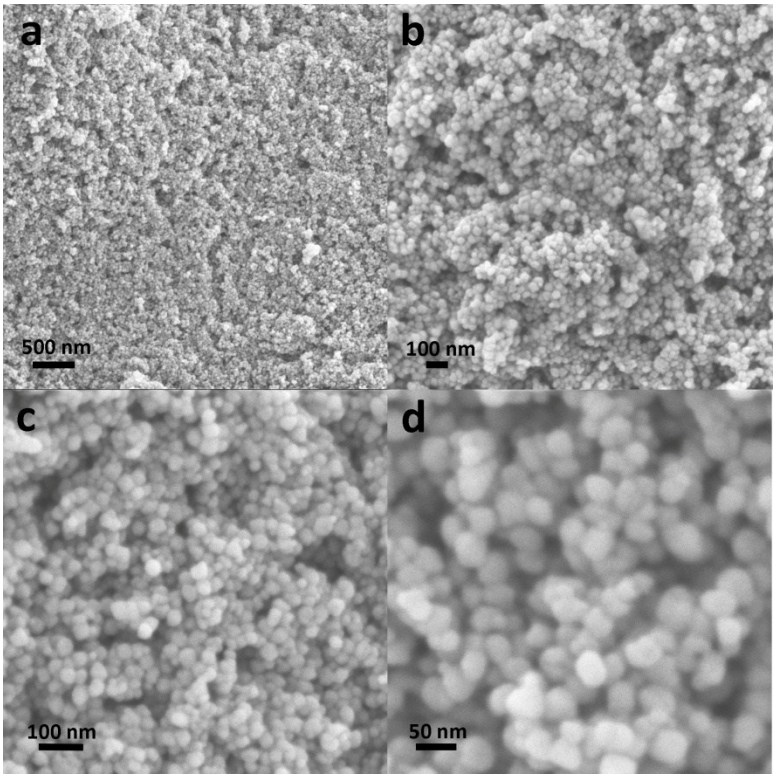

Fig. S9. SEM images of the as-prepared GDs-TiO_{2-x} hybrid.

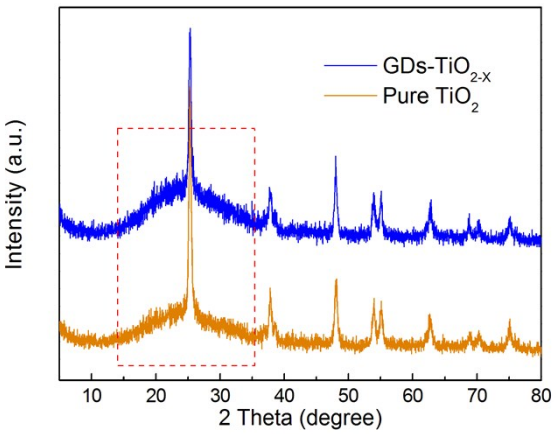

Fig. S10. XRD patterns of the as-prepared GDs-TiO_{2-x} and pure TiO_2.

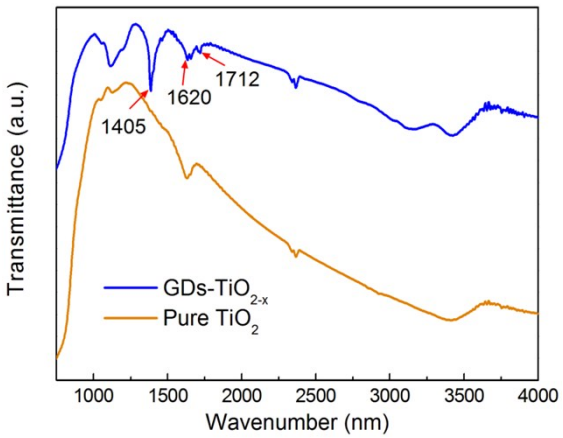

Fig. S11. FT-IR spectrum of the as-prepared GDs-TiO_{2-x} and pure TiO_2.

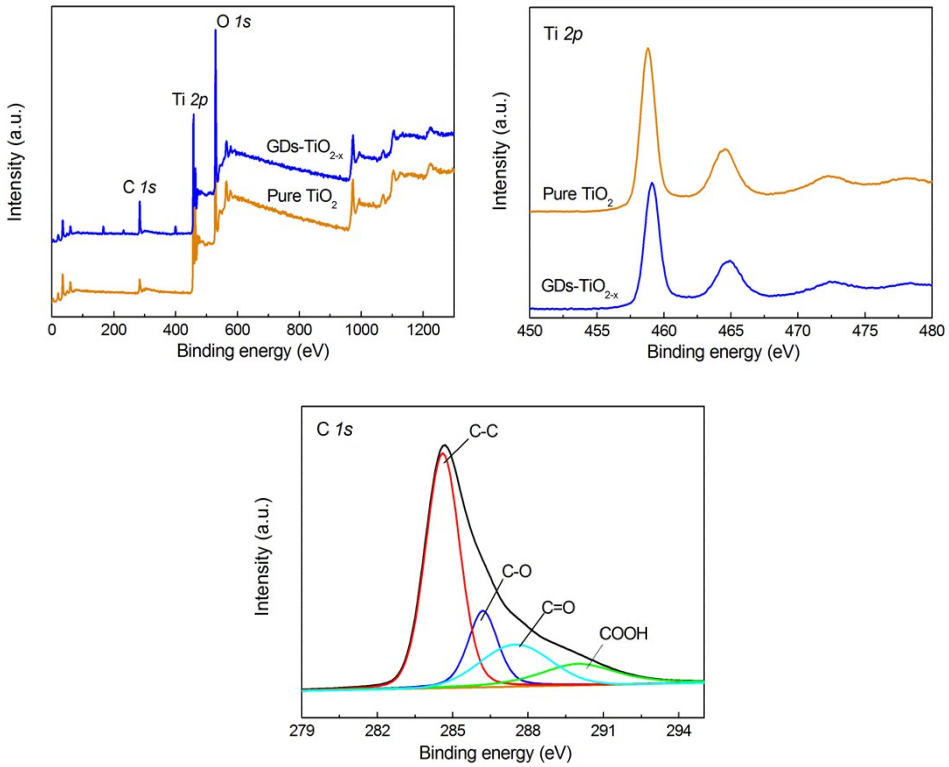

Fig. S12. XPS spectrum of the as-prepared GDs-TiO_{2-x} and pure TiO_2.

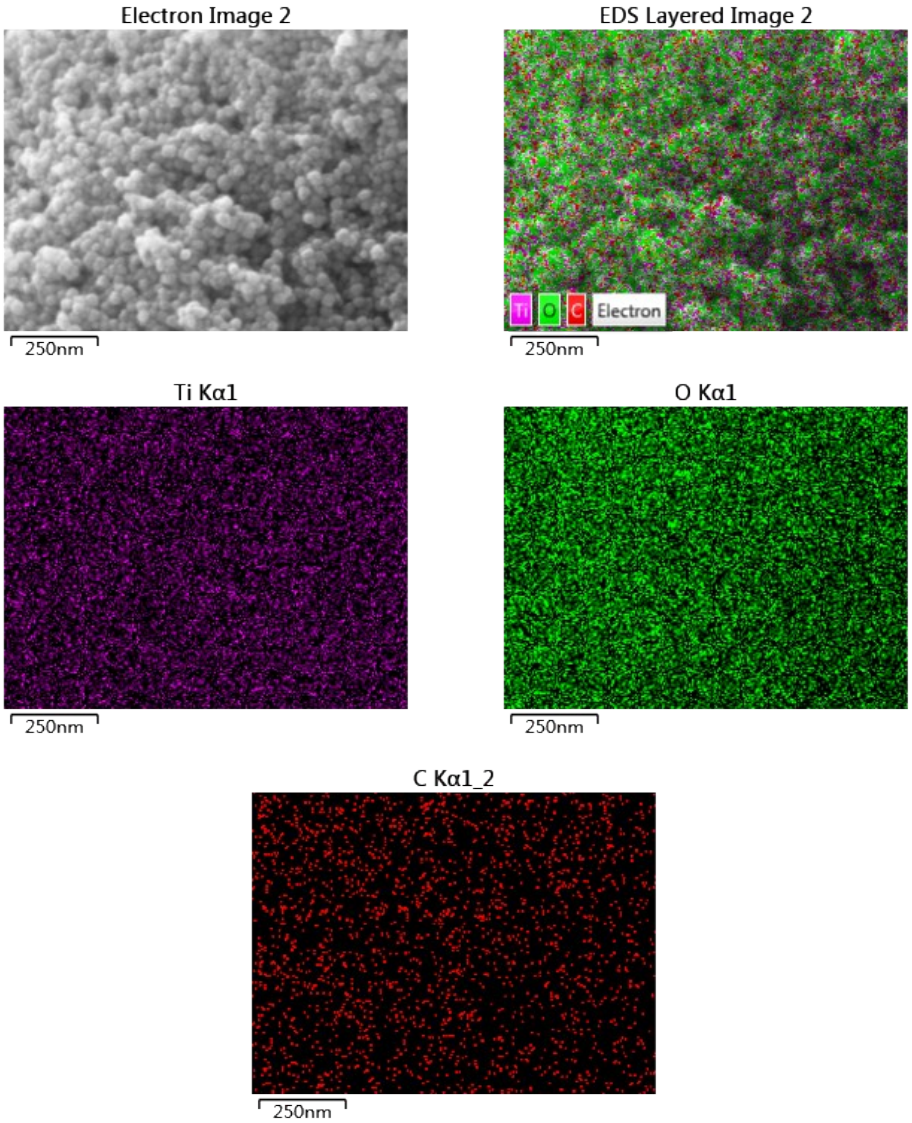

Fig. S13. EDX elemental mappings of the as-prepared GDs-TiO_{2-x}hybrid.

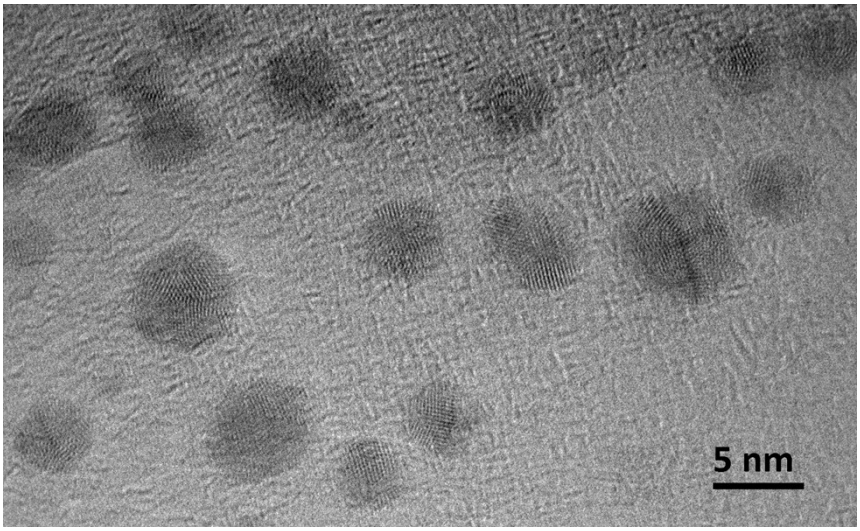

Fig. S14.TEM image of the as-prepared conventional GDs.

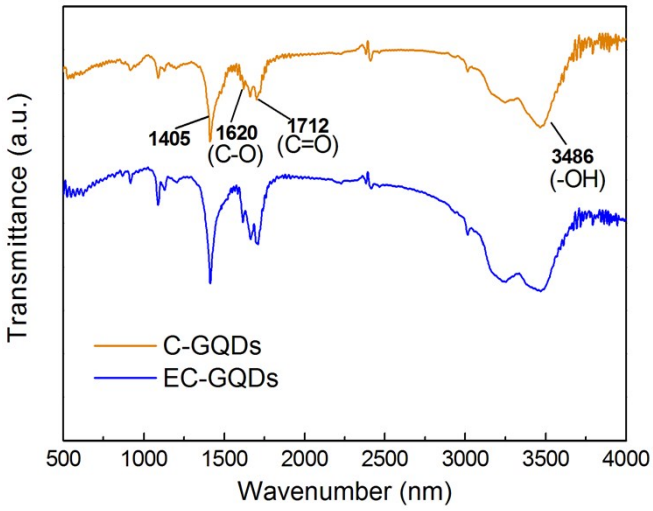

Fig. S15. FT-IR spectrum of the as-prepared EC-GDs and C-GDs.

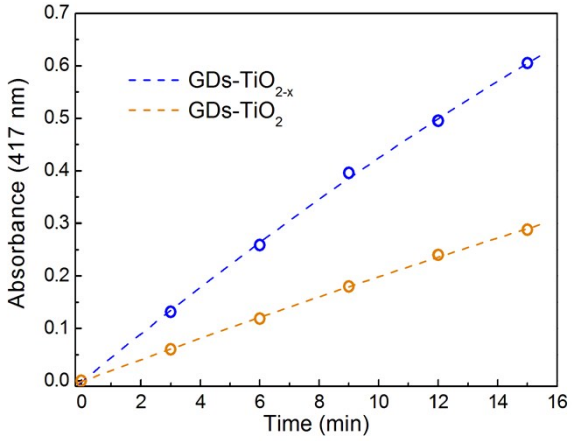

Fig. S16. Comparison of the •OH generation performance over GDs-TiO_{2-x} and GDs-TiO_2 catalyst.

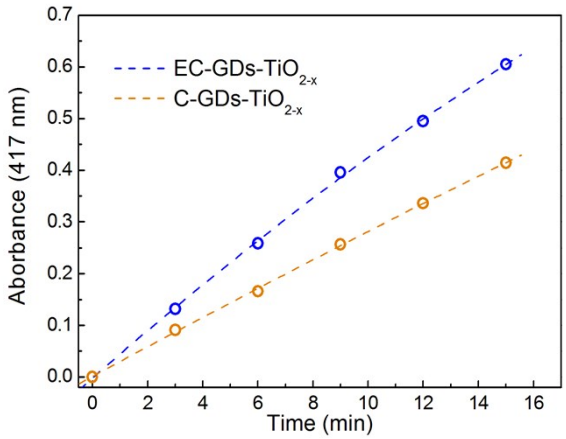

Fig. S17. Comparison of the •OH generation performance over EC-GDs-TiO_{2-x} and C-GDs-TiO_2 catalyst.

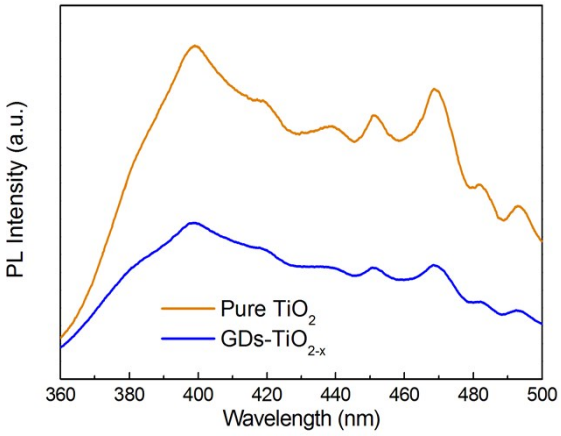

Fig. S18. PL spectrum of the as-prepared GDs-TiO_{2-x} hybrid and pure TiO_2.

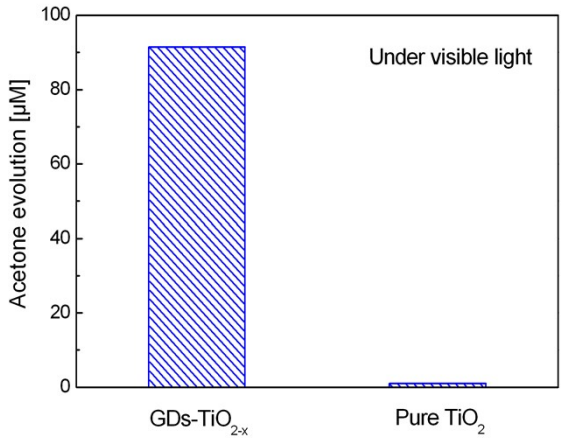

Fig. S19. Comparison of acetone evolution over different samples under visible-light irradiation.

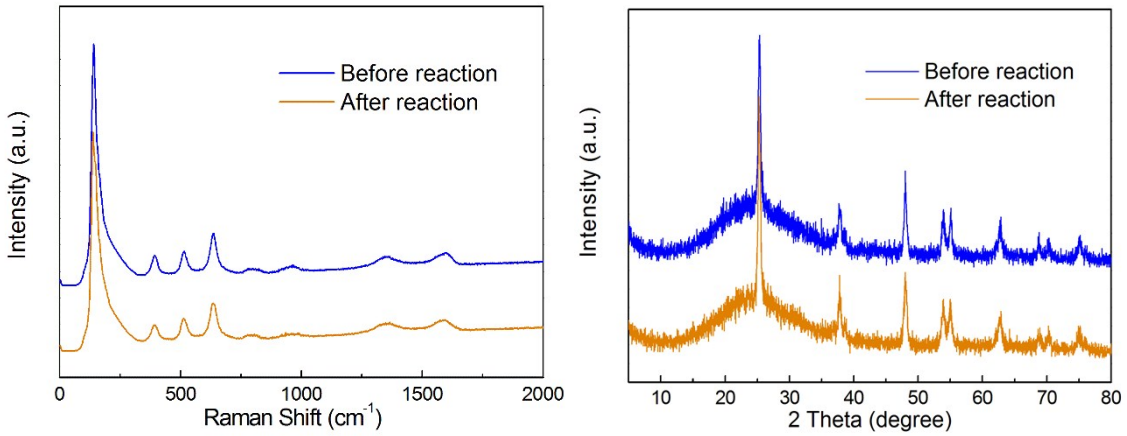

Fig. S20. The Raman spectrum and XRD patterns of GDs-TiO_{2-x} hybrid before and after photocatalytic degradation.

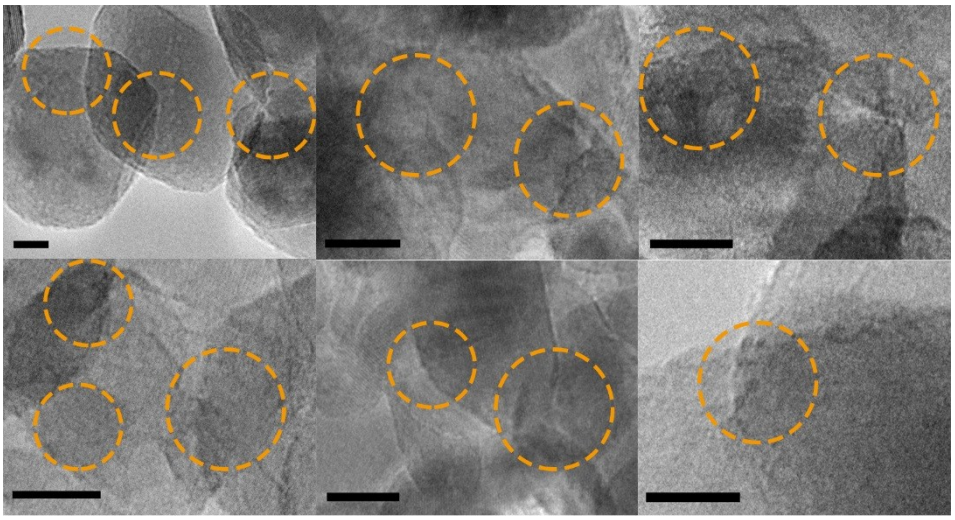

Fig. S21. The TEM images of the GDs-TiO_{2-x} after ten cycles photocatalytic experiments. The surface loaded GDs were marked by orange circles. Scale bars, 10 nm.

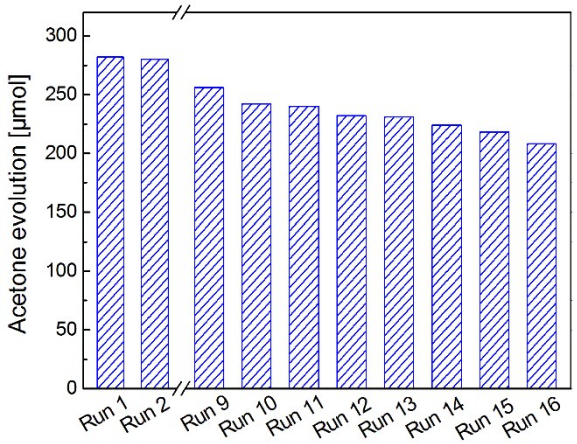

Fig. S22. Multi-cycle IPA photocatalytic degradation by using GDs-TiO_{2-x} as catalyst.

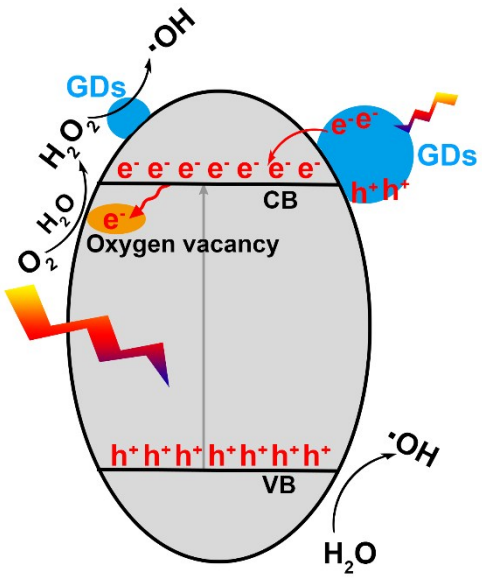

Fig. S23 Schematic illustrating the mechanism of the entire interfacial Fenton-like reaction.

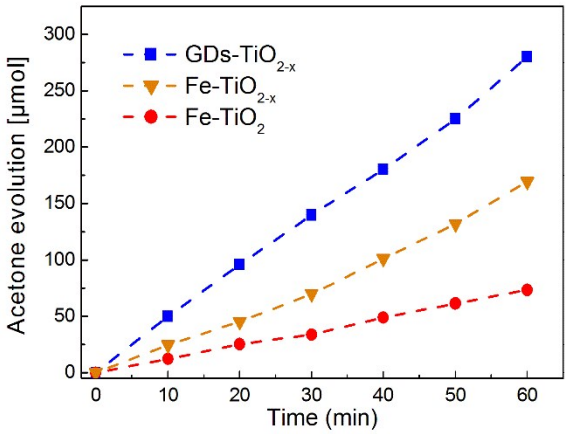

Fig. S24 Comparison of the photocatalytic activity over GDs-TiO_{2-x}, Fe-TiO_{2-x} and Fe-TiO_2.

In ordered to synthesis the Fe^{3+} modified TiO_2 or TiO_{2-x} catalysts, 60 mg of TiO_2 or TiO_{2-x} were first dispersed in 30 mL of distilled water. Dilute solution of $FeCl_3 \cdot 6H_2O$ (99.0%) was slowly added dropwise into the above solution. The weight of fraction of Fe^{3+} relative to TiO_2 or TiO_{2-x} are 1.4 wt%. The suspension was stirred for 24 h at room temperature and then dried at 80 °C for further photocatalytic experiments[14].

Table S1 Comparison of the photocatalytic activity of different samples with different GDs loading and oxygen vacancies concentration.

GDs (%) \ Solvent	**Water**	**Water/methanol=1:1**	**Methanol**
1.0 %	62 μmol/h	116 μmol/h	148 μmol/h
2.0 %	85 μmol/h	186 μmol/h	284 μmol/h
3.0 %	72 μmol/h	142 μmol/h	231 μmol/h

To ensure the optimal ratio between the surface oxygen defects and GDs for VOCs decomposition, we investigated the photooxidation performance of different samples with different GDs loading and O-vacancies concentration. In this experiment, we control the surface oxygen vacancies concentration of as-prepared sample via changing the solvents ratio between water and methanol (the methanol exhibits strong reduction ability during the hydrothermal reaction, and hence the different solvents ratio means different reduction ability) (Fig. 3b). Moreover, we also investigated the influence of GDs loading for photooxidation performance. As shown in Table S1, when the solvent is methanol and the GDs loading is 2.0% (wt%), the as-prepared sample exhibits the most excellent photooxidation performance.

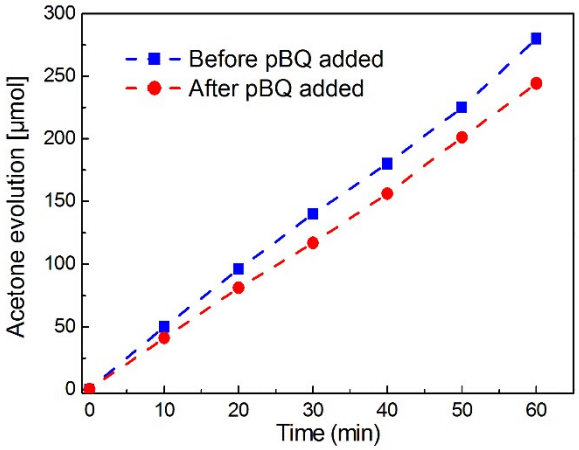

Fig. S25 Comparison of the photocatalytic activity of GDs-TiO_{2-x} before and after pBQ added.

To investigate the contribution of superoxide radicals generated by GDs-TiO_{2-x} for photocatalytic IPA removal, the capture experiments were performed. In this experiment, we use p-benzoquinone (pBQ) served as the scavengers for $\cdot O_2^-$, and the photocatalytic IPA degradation performance were compared and shown in Fig. S25. Clearly, after the pBQ were added in the reaction system, the photocatalytic performance exhibits a little decay, indicating the $\cdot O_2^-$ did not play an important role in IPA degradation.

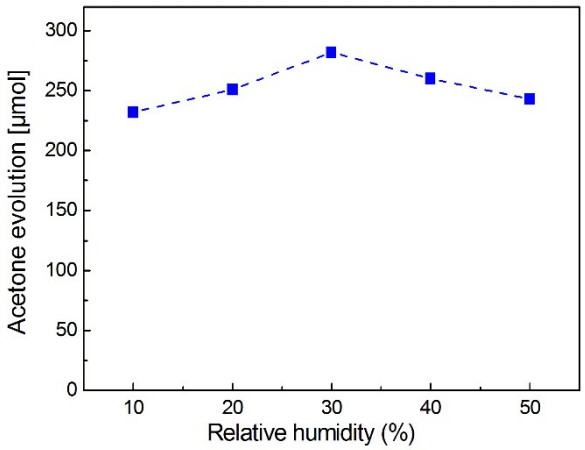

Fig. S26 Comparison of the photocatalytic activity of GDs-TiO_{2-x} under different relative humidity.

To investigate the influence of relative humidity for VOCs decomposition, we measured the photocatalytic activity of GDs-TiO_{2-x} catalyst under different environment humidity. As shown in Fig. S26, the photocatalyst exhibits the most excellent photocatalytic activity when the relative humidity is about 30%, which mainly owing the too low relative humidity cannot provide abundant reactant (H_2O) for photocatalytic VOC degradation, and the too high relative humidity is unbeneficial for the absorption of VOC on catalyst surface (the competitive adsorption effect from water).

Table S2 Graphene nanodots synthesis process under various reaction conditions.

Precursor	Reaction condition	Method	Reference
Graphite powder	Mixed with 20 mL of fuming HNO_3, followed by adding 100 mL of H_2SO_4 (98%) and stirred for 2 h at 110 °C.	Chemical oxidation	1
Carbon black	Refluxing carbon black powders with nitric acid (50 mL, 6 M) for 24 h.	Chemical oxidation	2
Carbon black	HNO_3 refluxed for 24 h at 110 ^oC .	Chemical oxidation	3
Graphene oxide	Sonicated in concentrated H_2SO_4 and HNO_3 for 10 h	Chemical oxidation	4
Carbon black	Mixed with 6 mL of fuming HNO_3, followed by adding 18 mL of H_2SO_4 and stirred at 160 °C.	Chemical oxidation	5
Graphene oxide	Mixed with concentrated HNO_3 and H_2SO_4, and refluxed under microwave irradiation for 9 h	Chemical oxidation	6
Graphene film	Cyclic voltammogramic scan performed in 0.1 M Na_2SO_4 solution by using graphene film as working electrode.	Electrochemical tailoring method	7
Graphite paper	Two graphite paper strips were inserted into water/ethanol solution, and a bias of 30 V was applied between the two electrodes.	Electrochemical tailoring method	This work

Table S3 Photocatalysis VOCs degradation performance of different catalysts under various reaction conditions.

Samples	Pollutant	Reaction Conditions	Product Yield (mol/h)	Reference
g-C_3N_4/WO_3	CH_3CHO	100 mg catalyst, LED lamp, λ= 435 nm	CO_2, 0.9	8
g-C_3N_4/TiO_2	HCHO	300 mg catalyst, UV lamp	CO_2, 2.8	9
P25	$(CH_3)_2CHOH$	50 mg catalyst, 300 W Xe lamp (AM 1.5)	CO_2, 2.5	10
N-TiO_2	$(CH_3)_2CHOH$	50 mg catalyst, 300 W Xe lamp (AM 1.5)	CO_2, 2.1	10
g-C_3N_4/Bi_2O_3	$(CH_3)_2CHOH$	50 mg catalyst, 300 W Xe lamp, 420 nm ≤ λ ≤ 800 nm	Acetone, 8.9	11
CNK-OH&Fe	$(CH_3)_2CHOH$	50 mg catalyst, 300 W Xe lamp (AM 1.5)	CO_2, 6.1	10
CeO_2-TiO_2	C_7H_8	40 mg catalyst, Simulated sunlight	CO_2, 1.26	12
C_3N_4-TiO_2	C_7H_8	40 mg catalyst, Simulated sunlight	CO_2, 0.648	13
GDs-TiO_{2-x}	C_7H_8	50 mg catalyst, 300 W Xe lamp (AM 1.5)	CO_2, 5.47	**This work**
GDs-TiO_{2-x}	$(CH_3)_2CHOH$	50 mg catalyst, 300 W Xe lamp (AM 1.5)	CO_2, 13	**This work**

References

1. Y. Chong, C. C. Ge, G. Fang, X. Tian, X. C. Ma, T. Wen, W. G. Wamer, C. Y. Chen, Z. F. Chai, J. J. Yin, *ACS Nano*, 2016, 10, 8690.
2. N. Li, A. Than, X. W. Wang, S. H. Xu, L. Sun, H. W. Duan, C. J. Xu, P. Chen, *ACS Nano*, 2016, 10, 3622.
3. Z. P. Zeng, F. X. Xiao, X. C. Gui, R. Wang, B. Liu, T. Tan, *J. Mater. Chem. A*, 2016, 4, 16383.
4. Y. T. Liang, C. G. Lu, D. F. Ding, M. Zhao, D. W. Wang, C. Hu, J. S. Qiu, G. Xie, Z. Y. Tang, *Chem. Sci.***,** 2015, 6, 4103.
5. S. J. Wang, I. S. Cole, Q. Li, *Chem. Commun.***,** 2016**,** 52**,** 9208**.**
6. H. J. Sun, N. Gao, K. Dong, J. S. Ren, X. G. Qu, *ACS Nano*, 2014, 8, 6202.
7. Y. Li, Y. Hu, Y. Zhao, G. Q. Shi, L. E. Deng, Y. B. Hou, L. T. Qu, *Adv. Mater.,* 2011, 23, 776.
8. Z. Y. Jin, N. Murakami, T. Tsubota, T. Ohno, *Appl. Catal. B-Environ.* 2014, 150-151, 479.
9. J. G. Yu, S. H. Wang, J. X. Low, W. Xiao, *Phys. Chem. Chem. Phys*., 2013, 15, 16883.
10. Y. X. Li, S. X. Ouyang, H. Xu, X. Wang, Y. P. Bi, Y. F. Zhang, J. H. Ye, *J. Am. Chem. Soc.*, 2016, 138, 13289–13297
11. Jiang, H. Y.; Liu, G. G.; Wang, T.; Li, P.; Lin, J.; Ye, J. H. *RSC Adv*., 2015, 5, 92963.
12. M. J, Muñoz-Batista, M. Fernández-García, A. Kubacka, *Appl. Catal. B-Environ.,* 2015, 164, 261.
13. M. J. Muñoz-Batista, A. Kubacka, M. Fernández-García, *Catal. Sci. Technol.*, 2014, 4, 2006
14. Y. X. Li, S. X. Ouyang, H. Xu, X. Wang, Y. P. Bi, Y. F. Zhang, J. H. Ye, *J. Am. Chem. Soc.*, 2016, 138, 13289.